Automated segmentation method of white matter and gray matter regions with multiple sclerosis lesions in MR images

Magome, Taiki
Japan Society for the Promotion of Science

Arimura, Hidetaka
Department of Health Sciences, Faculty of Medical Sciences, Kyushu University

Kakeda, Shingo
Department of Radiology, University of Occupational and Environmental Health, School of Medicine

Yamamoto, Daisuke
Department of Health Sciences, Graduate School of Medical Sciences, Kyushu University

他

出版情報：Radiological Physics and Technology. 4 (1), pp.61-72, 2011-01. Springer Japan
バージョン：

Automated segmentation method of white matter and gray matter regions with multiple sclerosis lesions in MR images

Taiki Magome・Hidetaka Arimura・Shingo Kakeda・Daisuke Yamamoto・
Yasuo Kawata・Yasuo Yamashita・Yoshiharu Higashida・Fukai Toyofuku・
Masafumi Ohki・Yukunori Korogi

T Magome・D Yamamoto・Y Kawata・Y Yamashita
Department of Health Sciences, Graduate School of Medical Sciences, Kyushu University, 3-1-1, Maidashi, Higashi-ku, Fukuoka 812-8582, Japan

T Magome
Research Fellow of the Japan Society for the Promotion of Science

H Arimura (Corresponding author)・Y Higashida・F Toyofuku・M Ohki
Department of Health Sciences, Faculty of Medical Sciences, Kyushu University, 3-1-1, Maidashi, Higashi-ku, Fukuoka 812-8582, Japan
e-mail: arimura@shs.kyushu-u.ac.jp

S Kakeda・Y Korogi
Department of Radiology, University of Occupational and Environmental Health, School of Medicine, 1-1, Iseigaoka, Yahatanishi-ku, Kitakyushu 807-8555, Japan

Present Address:
D Yamamoto
Siemens Corporation, Tokyo 141-8641, Japan

Present Address:
Y Kawata
Hitachi Medical Corporation, Kashiwa 277-0804, Japan

An abbreviated title:

Segmentation of white matter and gray matter

Abstract

Our purpose in this study was to develop an automated method for segmentation of white matter (WM) and gray matter (GM) regions with multiple sclerosis (MS) lesions in magnetic resonance (MR) images. The brain parenchymal (BP) region was derived from a histogram analysis for a T1-weighted image. The WM regions were segmented by use of addition of MS candidate regions, which were detected by our computer-aided detection system for the MS lesions, and subtraction of a basal ganglia and thalamus template from "tentative" WM regions. The GM regions were obtained by subtraction of the WM regions from the BP region. We applied our proposed method to T1-weighted, T2-weighted, and fluid-attenuated inversion-recovery (FLAIR) images acquired from 7 MS patients and 7 control subjects on a 3.0 T MRI system. The average similarity indices between the specific regions obtained by our method and by neuroradiologists for the BP and WM regions were 95.5 ± 1.2% and 85.2 ± 4.3%, respectively, for MS patients. Moreover, they were 95.0 ± 2.0% and 85.9 ± 3.4%, respectively, for the control subjects. The proposed method might be feasible for segmentation of WM and GM regions in MS patients.

Keywords Multiple sclerosis・Segmentation・Level set method・White matter・Gray matter

1 Introduction

Multiple sclerosis (MS) is a neurological disorder in the central nervous system. The progressive development of brain atrophy is a well-known characteristic of MS and is viewed as a potential marker of brain damage [1-7]. Therefore, the quantitative evaluation of brain atrophy is important for diagnosis or follow-up of MS by use of magnetic resonance (MR) imaging. Previous MR studies have shown that white matter atrophy in patients with primary progressive MS was closely related to clinical outcome [8], and gray matter atrophy in relapsing-remitting MS (RRMS) was related to the Expanded Disability Status Scale [9]. In such studies, neuroradiologists need to segment the brain parenchyma into the white matter and gray matter regions. However, it is laborious for neuroradiologists to determine the atrophies of the white matter and gray matter regions in MR images on a slice-by-slice basis. Therefore, a number of semi-automated and automated methods for segmentation of the white matter and gray matter regions have been developed for assisting radiologists in evaluating the atrophies of these regions in clinical practice [10-19]. However, these methods were developed for MR images without MS lesions. Ge et al. [2] proposed a semi-automated method based on fuzzy connectedness [10] for segmentation of white matter and gray matter regions with MS lesions. Stefano et al. [5] developed a semi-automated method by using the SIENA (structural imaging evaluation of normalized atrophy) X software [20] for segmentation of cortical gray matter regions with MS lesions.

In general, semi-automated methods are time-consuming, and the results depend on how the methods are used. Alfano et al. [11,21] developed an automated method for extraction of the white matter and gray matter regions in MS patients for estimation of their atrophy, although they did not evaluate the accuracy of their segmentation method. Many researchers employed statistical parametric mapping (SPM99) [12] as an automated segmentation tool for

78 the white matter and gray matter regions [3,6-9]. However, a majority of MS lesions in the
79 white matter regions were misclassified as gray matter or cerebrospinal fluid (CSF) by SPM99.
80 Therefore, further studies are still required for automatically segmenting the white matter and
81 gray matter regions including MS lesions for more accurate evaluation of the atrophies in both
82 regions in MS patients. That is because the atrophy in the white matter regions cannot be
83 correctly evaluated if the MS lesions in the white matter regions are not included. Our purpose
84 in this study was to develop an automated method for segmentation of the white matter and gray
85 matter regions including MS lesions in MR images.
86
87 **2 Materials and methods**
88
89 2.1 Clinical cases
90
91 The MR images of seven patients with RRMS and seven normal controls were used
92 for this study. Patients who were diagnosed as having MS and had MR examinations from
93 January 2007 to April 2008 were sequentially selected. Non-MS subjects, who were matched
94 with the MS patients in terms of age and gender, were chosen as control cases from all non-MS
95 patients who had MR examinations from January 2007 to March 2007. The MS group (5
96 females and 2 males) had a mean age of 31 years (range: 24-51 years), and the control group (5
97 females and 2 males) had a mean age of 30 years (range: 15-56 years). This study was
98 performed under a protocol approved by the institutional review board of the university
99 hospital.
100 All brain MR images were acquired with a 3.0 Tesla MR system (Signa Excite; GE
101 Medical systems, Milwaukee, Wis, USA). The following three imaging parameters were used:
102 2500/9.1/1000/224×320/2/1 minute 30 seconds [repetition time msec/echo time msec/inversion

time/matrix size/number of excitations (NEX)/imaging time] for each two-dimensional (2D) T1-weighted spin-echo imaging, 4000/85/512×312/3/10.9/3 minutes 20 seconds (repetition time msec/echo time msec/matrix size/NEX/echo-spacing/imaging time) for each 2D T2-weighted fast spin-echo imaging, and 12000/140/2600/224×256/2/9.1/3 minutes 20 seconds (repetition time msec/echo time msec/inversion time/matrix size/NEX/echo-spacing/imaging time) for each 2D fluid-attenuated inversion-recovery (FLAIR) imaging. All images were acquired with a section thickness of 5 mm, an intersection gap of 1 mm, a field of view of 22 cm, and 16-bit gray levels. Zero-fill interpolation processing was used for reconstruction of 2D images with 512 × 512 pixels and a pixel size of 0.4297 mm, which result in apparent high resolution images.

Three slices, which were located at the basal ganglia or at more superior levels, were selected per case, because Carone et al. [7] had reported that the basal ganglia, thalamus, and superior cortex were atrophied in MS patients.

2.2 Segmentation of brain parenchymal regions

The brain parenchymal region was segmented from a T1-weighted image based on an analysis of a gray-level histogram [22]. Figure 1 shows an example of a histogram of an original T1-weighted image. The histogram of a T1-weighted image can be divided into four parts, i.e., background, CSF, brain parenchymal, and fat regions. First, the head region was extracted from the original T1-weighted image by use of the threshold value T_{BG} given by

$$T_{BG} = M_{BG} + k_{BG} SD_{BG}, \qquad (1)$$

where M_{BG} and SD_{BG} are the mean value and the standard deviation (SD), respectively, determined from the first largest peak (the first left peak) with more than a certain number of pixels in the histogram as shown in Fig. 1, which was empirically set as 10,000 pixels in this

study. k_{BG} is a constant. Second, the CSF regions were removed from the head region with the threshold value T_{CSF} obtained by an automated thresholding technique based on linear discriminant analysis [23] for the histogram of the T1-weighted image. Third, the brain parenchymal region was extracted by reduction of the fat regions in a manner similar to that for the background. The threshold value for the fat region T_{FAT} was determined by

$$T_{FAT} = M_{BP} + k_{BP} SD_{BP}, \quad (2)$$

where M_{BP} and SD_{BP} are the mean value and the standard deviation, respectively, obtained from the second largest peak (the first right peak) with more than a certain number of pixels in the histogram of the brain parenchymal and fat regions as shown in Fig. 1, which was empirically set as 700 pixels in this study. k_{BP} is a constant. Note that some small holes could occur within the brain parenchymal region, because a number of pixels in the brain parenchymal region are similar to those in the fat regions. Therefore, the holes were filled in by the addition of a rough brain parenchymal region without holes to the brain parenchymal region after reduction of the fat region. The rough brain parenchymal region without holes was obtained by application of a circular morphological erosion kernel to the head region. In this study, the constant values k_{BG} and k_{BP} were set as 10 and 4, respectively. The parameters were determined empirically by use of nine clinical cases in the study of Kawata et al. [22], which are different from cases used in this study.

2.3 Segmentation of white matter regions

Figure 2 shows the overall scheme for segmentation of the white matter regions. First, a brain parenchymal region was segmented by use of the method mentioned above. Second, a T2-T1 subtraction image was obtained by subtraction of a T1-weighted image from a T2-weighted image. Third, the “tentative” white matter regions were segmented on the

153 subtraction image by use of a level set method [24] in the brain parenchymal region. Fourth, MS
154 candidate regions detected by our computer-aided detection (CAD) system [25] were added
155 onto the "tentative" white matter regions. Fifth, the white matter regions were determined by
156 removal of a basal ganglia and thalamus (BGT) template from the white matter regions.
157
158 *2.3.1 Subtraction image between T2-weighted and T1-weighted images*
159
160 A T1-weighted image was subtracted from a T2-weighted image for increasing the
161 contrast between the white matter and gray matter regions. Figure 3 shows the three pixel value
162 histograms of the brain parenchymal region in T2-weighted, T1-weighted, and subtraction
163 images, whose pixel values were normalized from 0 to 1023. In the T2-weighted image, the
164 white matter regions have lower pixel values compared with the gray matter regions, whereas
165 there is an inverse relationship in the T1-weighted image. On the other hand, the contrast could
166 not be detected in the T1-weighted images, because the peaks of the white matter and gray
167 matter regions were overlapped. The average contrast between the peak pixel values of the
168 white matter and gray matter regions for 14 slices selected from 14 cases was 174 ± 53.7 pixel
169 values for the subtraction images, and 119 ± 21.3 pixel values for the T2-weighted images. As a
170 result, the white-matter-gray-matter contrast in the subtraction image was higher than that in the
171 T2-weighted image with a statistically significant difference ($P < 0.01$). Therefore, the contrast
172 between the white matter and gray matter regions was increased by subtraction of the
173 T1-weighted image from the T2-weighted image. Figure 4 shows the brain parenchymal regions
174 in three images, i.e., T2- weighted, T1-weighted, and the T2-T1 subtraction image. The T2-T1
175 subtraction image seems to have the highest contrast.
176
177 *2.3.2 Segmentation of initial white matter regions*

178

179 The initial white matter candidate regions were segmented from the T2-T1 subtraction
180 image by use of an automated thresholding technique based on a linear discriminant analysis
181 [23] for a pixel value histogram in the brain parenchymal region. However, a number of thin
182 and long fat regions as well as the small white matter regions were still remained. Therefore,
183 two types of candidate regions were selected as the white matter regions. One type was the
184 candidate region of the largest size, and the other type was a region whose mean pixel value was
185 within the range between the mean pixel value ± a SD of the largest region. Finally, a
186 morphological erosion operation with a 3×3 kernel was applied three times to the binary image
187 with white matter candidate regions on the assumption that the eroded regions could be inside
188 the "true" white matter regions. The resulting white matter candidate regions were considered as
189 initial white matter regions.

190

191 *2.3.3 Segmentation of "tentative" white matter regions based on a level set method*

192

193 The "tentative" white matter regions were segmented based on a level set method,
194 where a new speed function was developed in this study for accurate segmentation of white
195 matter regions. The level set method is an active contour model, which has been widely used for
196 segmentation of some anatomical regions in medical images such as brain regions in MR
197 images [24,26,27]. In our research, the level set method was performed by means of a fast
198 narrow band method [28,29] for reducing the calculation time. First, a level set function ϕ was
199 determined as a signed distance function from the contour of the initial white matter regions,
200 which was the zero level in the level set function. Second, the level set function ϕ was updated
201 according to the following partial differential equation:

$$\frac{\partial \phi}{\partial t} + F\left|\nabla \phi\right| = 0, \quad (3)$$

where t is the time, F is the speed function, and ∇ is the gradient operator. While the level set function is updated, the zero level set ($\phi = 0$) moves according to the speed function in the three-dimensional (3D) level set function. Here, the zero level set is called a "moving front". Finally, the update of the level set function was stopped if a certain ratio of pixels r_t on the zero level did not move within a certain number of iterations i_t. The zero level ($\phi = 0$) of the function is considered as the final contour of the object. In this study, we developed a speed function F given by

$$F = b\left(v + \rho\kappa\right), \quad (4)$$

where b is the edge indicator function, v and ρ are constants, and κ is the mean curvature. The term of $\rho\kappa$ gives the smoothness of the front propagation. The edge indicator function b is defined as

$$b = \frac{1}{1 + \left|\nabla I(x, y)\right|}, \quad (5)$$

where $I(x, y)$ is the image processed with an adaptive partial median (APM) filter [30]. The edge indicator function b plays an important role for stopping the moving front propagation at the desired boundary of the object, because the function b approaches zero when the moving front arrives at the object boundary. However, if the object boundary includes noise, the segmentation result would be inaccurate and unstable. Therefore, some smoothing filter such as a Gaussian filter should be applied to the original image for reduction of noise prior to application of the level set method. However, an edge-preserving smoothing (EPS) filter would be preferred as a smoothing filter, because the general smoothing filters blur the edge of an object. In this study, we chose an APM filter developed by Lee et al. [30] as an EPS filter, because the APM filter can reduce noise with preserving edges owing to their adaptive filter size and shape in each pixel. Figure 5 shows an original T2-weighted image and resulting

images obtained by three smoothing filters, i.e., the Gaussian filter, an EPS filter [31], and the APM filter. The image processed with the APM filter seems to be the best among the three images in terms of reducing noise and preserving edges. In this study, the parameter values r_t, i_t, v, and ρ were set as 0.999, 500, 1.0, and -0.6, respectively, which were optimized so that the maximum similarity index (Eq. (6) in Subsection 2.5) could be obtained. The time interval for the partial differential equation was set as 0.1.

2.3.4 Addition of MS regions detected by a CAD system onto "tentative" white matter regions

MS candidate regions, which were automatically detected in the FLAIR image by a CAD system for MS developed by Yamamoto et al. [25], were added onto the "tentative" white matter regions, because several high-contrast MS lesions were not included in the white matter regions. Figure 6 shows an illustration of addition of MS regions detected by a CAD system for MS. As shown in this figure, the holes corresponding to MS regions in the "tentative" white matter regions were filled in by adding of the MS regions detected by a CAD system for MS.

Prior to the addition of MS regions, a morphological dilation operation with a 3×3-square kernel was applied to the MS candidate regions. At the end of this processing, a morphological closing operation with a 3×3-square kernel was applied three times to white matter candidate regions with MS candidate regions for smoothing of candidate regions.

The overall scheme for segmentation of MS regions is shown in Fig. 7. In the CAD system [25], MS candidate regions were detected through the following steps:

(1) MS lesions were enhanced by subtraction of a background image, which was approximated by the first order polynomial in the brain parenchymal region from the FLAIR image. (2) The initial candidates were identified by use of a multiple gray-level thresholding technique on the subtraction image as the points with local maximum pixel values [32,33]. MS candidate regions

were segmented by use of a region-growing technique from the location of the initial candidates based on monitoring of large changes in five image features, i.e., effective diameter, area, circularity, slenderness, and the difference in the mean pixel value within the inner and outer regions of a candidate region. (3) The large number of false positive regions was reduced based on a rule-based method. (4) Final regions in MS candidates were determined by use of a level set method, which was used for reduction of false positives as well as more accurate segmentation. (5) All candidate regions were classified into true positive and false positive candidate regions by use of a support vector machine, which is a classifier based on a statistical learning theory.

2.3.5 Removing of basal ganglia and thalamus from white matter candidate regions

Final white matter regions were determined by removal of a basal ganglia and thalamus template of the gray matter from the white matter regions, because it was difficult to remove the basal ganglia and thalamus regions of the gray matter from the white matter regions due to the very low contrast. The basal ganglia and thalamus template shown in Fig. 8 was produced manually from a T2-weighted image of one patient out of the 14 cases used in this study. The slices including the basal ganglia and thalamus were selected manually, and then the basal ganglia and thalamus template was adjusted to each brain parenchyma by use of a 2D affine transformation [34]. Finally, the white matter regions were determined after removal of the adjusted template from the tentative white matter regions. The nine feature points for the affine transformation were selected automatically on two straight lines that ran at right angles to one another, in the circumscribed rectangle of the brain parenchyma.

The internal capsules of the white matter were included in the basal ganglia and thalamus template, because it seems impossible even for neuroradiologists to extract the internal

276 capsules in the T1-weighted, T2-weighted, and FLAIR images. Therefore, the internal capsule
277 was included in the gold standard regions of gray matter in this study.
278
279 2.4 Segmentation of gray matter regions
280
281 The gray matter regions were obtained by subtraction of the white matter regions from
282 the brain parenchymal region.
283
284 2.5 Evaluation of segmentation accuracy
285
286 The segmentation accuracy of our method was evaluated by use of a similarity index
287 [35], which means the degree of similarity between the candidate region *C* obtained by our
288 method and the gold standard region *G* obtained by a manual method. The similarity index was
289 obtained by the following equation:

290 $$Similarity\ index\ (\%) = \frac{2n\left(G \cap C\right)}{n\left(G\right) + n\left(C\right)} \times 100, \quad (6)$$

291 where $n(G)$ was the number of gold standard pixels, $n(C)$ was the number of segmented
292 pixels automatically determined by use of our method, and $n(G \cap C)$ was the number of
293 logical AND pixels between *G* and *C*. We defined the gold standard regions based on manual
294 contouring by an experienced neuroradiologist, following verification by a senior experienced
295 neuroradiologist. The gold standard regions of the brain parenchyma and white matter were
296 determined by the neuroradiologist's delineating their contours on the T1-weighted image and
297 T2-weighted image, respectively. Moreover, the gold standard regions of gray matter were
298 obtained by subtraction of the white matter regions from brain parenchymal regions. Therefore,
299 we evaluated the segmentation accuracy of the brain parenchymal and white matter regions by

using the similarity index. However, the variability of the gold standard was not investigated in this study, but is clarified in the Discussion Section.

3 Results

We investigated the computational impact of the CAD step on the proposed method. Results were obtained by use of a personal computer with two 2.66 GHz Intel Dual-Core Xeon CPUs and 5 GB memory. It took about 20 seconds and 150 seconds on average for the segmentation step and the CAD step to deal with each MR image, respectively. Therefore, the computational impact of the CAD step on the proposed method was 88% on average.

Table 1 shows the average similarity indices of all steps for the white matter regions. The average similarity indices for white matter regions without and with addition of MS candidate regions to the "tentative" white matter regions were 80.3 ± 10.3% and 80.5 ± 10.5%, respectively, in MS patients. According to these average results, the addition of MS candidate regions does not seem to be effective for accurate segmentation of the white matter regions. However, Fig. 9 shows a good example of the effect of adding MS candidate regions, i.e., segmented white matter regions of an MS patient without and with adding of MS candidate regions. The similarity index for the white matter regions increased from 84.7% to 89.3% by use of the proposed CAD system. The average similarity index for white matter regions increased from 80.5 ± 10.5% to 85.2 ± 4.3% in MS patients by removal of the basal ganglia and thalamus template region from the "tentative" white matter regions. Figure 10 shows two images, which are the white matter regions of an MS patient without and with removal of the basal ganglia and thalamus template region, respectively. The similarity index for the white matter regions increased from 68.2% to 84.0%. Furthermore, the average similarity index for white matter regions increased from 81.0 ± 9.8% to 85.9 ± 3.4% in the control subjects, and

increased from 80.7 ± 9.9% to 85.5 ± 3.8% in all cases by removal of the basal ganglia and thalamus template region.

As a final result, Fig. 11 shows the similarity indices for white matter and gray matter regions of all slices, and Table 2 shows the average similarity indices for the brain parenchymal and white matter regions. The average similarity indices of brain parenchymal and white matter regions were 95.5 ± 1.2% and 85.2 ± 4.3%, respectively, for MS patients. Moreover, they were 95.0 ± 2.0% and 85.9 ± 3.4%, respectively, for the control subjects. Here, there were no significant differences in the segmentation accuracy of any regions between MS patients and controls ($P > 0.35$). In all cases, the average similarity index was 95.2 ± 1.6% for brain parenchymal regions and 85.5 ± 3.8% for white matter regions. Examples of regions segmented by the proposed method are shown in Fig. 12. The similarity index was 95.9% for the brain parenchymal region and 85.7% for white matter regions.

4 Discussion

The proposed method is based on three kinds of 2D MR images, because (1) the T2-weighted and/or FLAIR 2D images have been established as routine sequences for diagnosis of MS lesions [36-38], (2) the data acquisition time of a 2D MR image is shorter than that of a 3D image, and (3) the in-plane spatial resolution and contrast in a 2D MR image can be higher than those of a 3D image, respectively. Nevertheless, there are a number of advantages of 3D imaging for accurate diagnosis of MS, such as identification of 3D locations of MS lesions and more accurate segmentation. The 3D locations of MS lesions are associated with visual, motor, and sensory impairments. Therefore, we plan to modify the proposed method from the 2D-based method to a 3D-based one.

The segmentation accuracy depends on the strength of the magnetic field. In this study,

350 all MR images were acquired on a 3.0 Tesla MR system. In general, lower magnetic field
351 strength increases the image noise, which could lead to inaccurate segmentation results.
352 Therefore, we should investigate the robustness of the proposed method by applying it to MR
353 images acquired on 1.5 Tesla or lower field MR systems in future work.

354 There is a chance that false positive candidates were included in initial white matter
355 regions as well as final white matter regions. As a result, however, there were 47 false positive
356 regions in all 42 slices used in this study, and thus the area ratio of the false positive regions to
357 the gold standard white matter regions was 0.17 ± 0.44% on average for each slice. Although
358 the number of false positive regions should be reduced as much as possible, there is little impact
359 of false positives on the segmentation accuracy in the proposed method.

360 It would be important to evaluate MS candidate regions that were underestimated and
361 overestimated by the proposed method at each step of the segmentation of white matter regions.
362 For that purpose, we calculated an overlap fraction (OF) and extra fraction (EF) [39], which can
363 evaluate underestimated and overestimated regions, respectively. The OF and EF are defined as

364 $$Overlap\ fraction(\%) = \frac{TP}{TP + FN} \times 100 , \quad (7)$$

365 $$Extra\ fraction(\%) = \frac{FP}{TP + FN} \times 100 , \quad (8)$$

366 where TP, FP, and FN are true positive, false positive, and false negative pixels, respectively.
367 The OF approaches unity with decreasing underestimated regions, whereas the EF approaches
368 zero with decreasing overestimated regions. For MS patients, the average OFs for white matter
369 regions without and with addition of CAD outputs were 89.2 ± 6.1% and 90.5 ± 5.1%,
370 respectively, and the average EFs were 35.7 ± 27.8% and 37.6 ± 29.1%, respectively. In this
371 step, some MS regions were removed as FNs, but also some FP regions were added onto the
372 white matter regions. Furthermore, for MS patients, the average OFs for white matter regions
373 without and with removal of the basal ganglia and thalamus regions were 90.5 ± 5.1% and 89.8

± 5.4%, respectively, and the average EF decreased from 37.6 ± 29.1% to 21.1 ± 8.7% ($P < 0.05$). On the other hand, for control subjects, the average OFs without and with removal of the basal ganglia and thalamus regions were 88.7 ± 3.7% and 88.2 ± 4.3%, respectively, and the average EF decreased from 33.0 ± 26.2% to 17.4 ± 7.1% ($P < 0.05$). Consequently, the average OF and EF in all cases were 89.0 ± 4.9% and 19.2 ± 8.1%, respectively, in the final step of the segmentation of white matter regions.

Although the gold standard regions for the brain parenchyma, white matter, and gray matter regions were based on manual contouring with the consensus of two experienced neuroradiologists in this study, it is important to consider inter- and intra-observer variability when the gold standard regions are determined by manual segmentation. Gao et al. [40] reported that there was intra-observer variability (maximum SD ranging from 2% to 8% of the mean) and inter-observer variability (SD of the observers' means being 18.8% of the mean volume) in the manual delineation of prostate volume on a computed tomography (CT) image for radiation therapy. The variability in the delineation of the white matter and gray matter could be larger than that of the prostate due to their complicated shapes. Therefore, we should investigate the variability of manual segmentation for white matter and gray matter regions by several observers, and then calculate the similarity index by considering the variability of the gold standards in future work.

Other limitations of this study need to be described. First, the CAD system for detection of MS regions [25] produced a few false positives, and it was not able to detect a number of MS regions. According to a report by Yamamoto et al. [25], the sensitivity and the number of false positives were 81.5% and 2.9, respectively, for 3 MS cases including 168 MS lesions, two cases of which were used for this study. The false positives and false negatives could lead to the overestimation and underestimation of white matter regions, respectively. Therefore, the CAD system should be improved in terms of the detection accuracy. Second, we

399 did not deal with cases where MS lesions were developed in the gray matter regions which were
400 reported by Kidd et al. [41] and Peterson et al. [42]. However, the current proposed method
401 considers all MS lesions as a part of the white matter regions [1-8], because the majority of MS
402 lesions develop in the white matter regions. Nonetheless, we should improve the proposed
403 method so that MS lesions detected by the CAD system can be classified correctly in the white
404 matter and gray matter regions.
405
406 **5 Conclusions**
407
408 We have developed an automated method for segmentation of the white matter and
409 gray matter regions including the MS lesions. As a result, the white matter and gray matter
410 regions are segmented automatically even if patients have MS lesions. Therefore, our proposed
411 method might be feasible as a diagnostic tool for MS patients in clinical practice.
412
413 **Acknowledgments**
414
415 The authors are grateful to Dr. Toshiaki Miyachi, Kanazawa University, for useful
416 suggestion, Dr. Junji Morishita, and Dr. Seiji Kumazawa, Kyushu University, for helpful
417 discussion.
418

References

1. Losseff NA, Wang L, Lai HM, Yoo DS, Gawne-Cain ML, McDonald WI, et al. Progressive cerebral atrophy in multiple sclerosis. A serial MRI study. Brain. 1996;119:2009-19.

2. Ge Y, Grossman RI, Udupa JK, Babb JS, Nyul LG, Kolson DL. Brain atrophy in relapsing-remitting multiple sclerosis: fractional volumetric analysis of gray matter and white matter. Radiology. 2001;220:606-10.

3. Chard DT, Griffin CM, Parker GJ, Kapoor R, Thompson AJ, Miller DH. Brain atrophy in clinically early relapsing-remitting multiple sclerosis. Brain. 2002;125:327-37.

4. Quarantelli M, Ciarmiello A, Morra VB, Orefice G, Larobina M, Lanzillo R, et al. Brain tissue volume changes in relapsing- remitting multiple sclerosis: correlation with lesion load. NeuroImage. 2003;18:360-6.

5. De Stefano N, Matthews PM, Filippi M, Agosta F, De Luca M, Bartolozzi ML, et al. Evidence of early cortical atrophy in MS Relevance to white matter changes and disability. Neurology. 2003;60:1157-62.

6. Dalton CM, Chard DT, Davies GR, Miszkiel KA, Altmann DR, Fernando K, et al. Early development of multiple sclerosis is associated with progressive grey matter atrophy in patients presenting with clinically isolated syndromes. Brain. 2004;127:1101-7.

7. Carone DA, Benedict RH, Dwyer MG, Cookfair DL, Srinivasaraghavan B, Tjoa CW, et al.

437 Semi-automatic brain region extraction (SABRE) reveals superior cortical and deep gray
438 matter atrophy in MS. NeuroImage. 2006;29:505-14.
439 8. Sastre-Garriga J, Ingle GT, Chard DT, Ramio-Torrenta L, Miller DH, Thompson AJ. Grey
440 and white matter atrophy in early clinical stages of primary progressive multiple sclerosis.
441 NeuroImage. 2004;22:353-9.
442 9. Sanfilipo MP, Benedict RH, Sharma J, Weinstock-Guttman B, Bakshi R. The relationship
443 between whole brain volume and disability in multiple sclerosis: a comparison of normalized
444 gray vs. white matter with misclassification correction. NeuroImage. 2005;26:1068-77.
445 10. Udupa JK, Samarasekera S. Fuzzy connectedness and object definition: theory, algorithms,
446 and applications in image segmentation. Graphical Models Image Process. 1996;58:246-61.
447 11. Alfano B, Brunetti A, Covelli EM, Quarantelli M, Panico MR, Ciarmiello A, et al.
448 Unsupervised, automated segmentation of the normal brain using a multispectral relaxometric
449 magnetic resonance approach. Magn Reson Med. 1997;37:84-93.
450 12. Ashburner J, Friston KJ. Voxel-based morphometry--the methods. NeuroImage.
451 2000;11:805-21.
452 13. Liu T, Li H, Wong K, Tarokh A, Guo L, Wong ST. Brain tissue segmentation based on DTI
453 data. NeuroImage. 2007;38:114-23.
454 14. Vrooman HA, Cocosco CA, van der Lijn F, Stokking R, Ikram MA, Vernooij MW, et al.

455 Multi-spectral brain tissue segmentation using automatically trained k-Nearest-Neighbor
456 classification. NeuroImage. 2007;37:71-81.
457 15. Hu Q, Qian G, Teistler M, Huang S. Informatics in radiology: automatic and adaptive brain
458 morphometry on MR images. Radiographics. 2008;28:345-56.
459 16. Lee H, Prohovnik I. Cross-validation of brain segmentation by SPM5 and SIENAX.
460 Psychiatry Res. 2008;164:172-7.
461 17. Chao WH, Chen YY, Lin SH, Shih YY, Tsang S. Automatic segmentation of magnetic
462 resonance images using a decision tree with spatial information. Comput Med Imaging Graph.
463 2009;33:111-21.
464 18. Klauschen F, Goldman A, Barra V, Meyer-Lindenberg A, Lundervold A. Evaluation of
465 automated brain MR image segmentation and volumetry methods. Hum Brain Mapp.
466 2009;30:1310-27.
467 19. Lee JD, Su HR, Cheng PE, Liou M, Aston JA, Tsai AC, et al. MR image segmentation
468 using a power transformation approach. IEEE Trans Med Imaging. 2009;28:894-905.
469 20. Smith SM, De Stefano N, Jenkinson M, Matthews PM. Normalized accurate measurement
470 of longitudinal brain change. J Comput Assist Tomogr. 2001;25:466-75.
471 21. Alfano B, Brunetti A, Larobina M, Quarantelli M, Tedeschi E, Ciarmiello A, et al.
472 Automated segmentation and measurement of global white matter lesion volume in patients

473 with multiple sclerosis. J Magn Reson Imaging. 2000;12:799-807.

474 22. Kawata Y, Arimura H, Yamashita Y, Magome T, Ohki M, Toyofuku F, et al.
475 Computer-aided evaluation method of white matter hyperintensities related to subcortical
476 vascular dementia based on magnetic resonance imaging. Comput Med Imaging Graph.
477 2010;34:370-6.

478 23. Otsu N. A threshold selection method from gray-level histograms. IEEE Trans Syst Man
479 Cybern. 1979;9:62-6.

480 24. Sethian JA. Level set methods and fast marching methods: evolving interfaces in
481 computational geometry, fluid mechanics, computer vision, and materials sciences.
482 Cambridge: Cambridge university press, 1999.

483 25. Yamamoto D, Arimura H, Kakeda S, Magome T, Yamashita Y, Toyofuku F, et al.
484 Computer-aided detection of multiple sclerosis lesions in brain magnetic resonance images:
485 False positive reduction scheme consisted of rule-based, level set method, and support vector
486 machine. Comput Med Imaging Graph. 2010;34:404-13.

487 26. Deng JW, Tsui HT. A fast level set method for segmentation of low contrast noisy
488 biomedical images. Pattern Recogn Lett. 2002;23:161-9.

489 27. Arimura H, Yoshiura T, Kumazawa S, Tanaka K, Koga H, Mihara F, et al. Automated
490 method for identification of patients with Alzheimer's disease based on three-dimensional

491 MR images. Acad Radiol. 2008;15:274–84.

492 28. Yui S, Hara K, Zha H, Hasegawa T. A fast narrow band method and its application in

493 topology-adaptive 3-D modeling. Int Conf Patt Recogn. 2002;4:122-5.

494 29. Iwashita Y, Kurazume R, Tsuji T, Hasegawa T, Hara K. Fast implementation of level set

495 method and its real-time applications. IEEE Int Conf on Syst Man Cybern. 2004;7:6302-7.

496 30. Lee Y, Takahashi N, Tsai D, Ishii K. Adaptive partial median filter for early CT signs of

497 acute cerebral infarction. Int J CARS. 2007;2:105-15.

498 31. Nagao M, Matsuyama T. Edge preserving smoothing. Comput Graph Image Process.

499 1979;9:394-407.

500 32. Arimura H, Katsuragawa S, Suzuki K, Li F, Shiraishi J, Sone S, et al. Computerized scheme

501 for automated detection of lung nodules in low-dose computed tomography images for lung

502 cancer screening. Acad Radiol. 2004;11:617-29.

503 33. Yamashita Y, Arimura H, Tsuchiya K. Computer-aided detection of ischemic lesions related

504 to subcortical vascular dementia on magnetic resonance images. Acad Radiol.

505 2008;15:978-85.

506 34. Hajnal JV, Hill DLG, Hawkes DJ. Medical image registration. USA: CRC Press, 2001.

507 35. Dice LR. Measures of the amount of ecologic association between species. Ecology.

508 1945;26:297-302.

509 36. McDonald WI, Compston A, Edan G, Goodkin D, Hartung HP, Lublin FD, et al.
510 Recommended diagnostic criteria for multiple sclerosis: Guidelines from the International
511 Panel on the Diagnosis of Multiple Sclerosis. Ann Neurol. 2001;50:121-7.
512 37. Filippi M, Rocca MA, Arnold DL, Bakshi R, Barkhof F, De Stefano N, et al. EFNS
513 guidelines on the use of neuroimaging in the management of multiple sclerosis. Eur J Neurol.
514 2006;13:313-25.
515 38. Simon JH, Li D, Traboulsee A, Coyle PK, Arnold DL, Barkhof F, et al. Standardized MR
516 imaging protocol for multiple sclerosis: Consortium of MS centers consensus guidelines. Am
517 J Neuroradiol. 2006;27:455-61.
518 39. Stokking R, Vincken KL, Viergever MA. Automatic morphology-based brain segmentation
519 (MBRASE) from MRI-T1 data. NeuroImage. 2000;12:726-38.
520 40. Gao Z, Wilkins D, Eapen L, Morash C, Wassef Y, Gerig L. A study of prostate delineation
521 referenced against a gold standard created from the visible human data. Radiother Oncol.
522 2007;85:239-46.
523 41. Kidd D, Barkhof F, McConnell R, Algra PR, Allen IV, Revesz T. Cortical lesions in
524 multiple sclerosis. Brain. 1999;122:17-26.
525 42. Peterson JW, Bo L, Mork S, Chang A, Trapp BD. Transected neurites, apoptotic neurons,
526 and reduced inflammation in cortical multiple sclerosis lesions. Ann Neurol.

527 2001;50:389–400.

528

529 **Table 1** Average similarity indices of all steps for white matter regions.

530

	MS patients (%)	Controls (%)	All cases (%)
Initial white matter	80.3 ± 10.3	81.0 ± 9.8	80.7 ± 9.9
Level set method	80.3 ± 10.3	81.0 ± 9.8	80.7 ± 9.9
Addition of MS regions	80.5 ± 10.5	-	-
Removal of BGT template	85.2 ± 4.3	85.9 ± 3.4	85.5 ± 3.8

531

532

533

534 **Table 2** Average similarity indices between regions obtained by the proposed method and
535 neuroradiologists for brain parenchymal, white matter, and gray matter regions.
536

	MS patients (%)	Controls (%)	*P* value	All cases (%)
Brain parenchyma	95.5 ± 1.2	95.0 ± 2.0	0.359	95.2 ± 1.6
White matter	85.2 ± 4.3	85.9 ± 3.4	0.572	85.5 ± 3.8

537
538

Figure legends

Fig. 1 Pixel value histogram of an original T1-weighted image, which has four parts corresponding to the background, CSF, brain parenchymal, and fat regions, respectively. T_{BG}, T_{CSF} and T_{FAT} are the threshold values for reducing the background, CSF, and fat regions, respectively.

Fig. 2 Overall scheme for segmentation of white matter (WM) regions.

Fig. 3 Pixel value histograms of a T2-weighted image (T2WI), a T1-weighted image (T1WI), and a T2-T1 subtraction image in the brain parenchymal region.

Fig. 4 Brain parenchymal regions in **a** T2-weighted image, **b** T1-weighted image, and **c** T2-T1 subtraction image.

Fig. 5 Comparison of results obtained by three smoothing filters: **a** an original image, **b** with a Gaussian filter, **c** with an edge-preserving smoothing filter, and **d** with an adaptive partial median filter.

Fig. 6 Illustration of addition of MS regions detected by a CAD system for MS onto "tentative" white matter regions: **a** MS candidate regions detected by a CAD system, **b** "tentative" white matter regions, where there were holes corresponding to MS regions, **c** "tentative" white matter regions, where the holes were filled in by adding of the MS regions.

Fig. 7 Overall scheme for segmentation of MS regions.

Fig. 8 A template with basal ganglia and thalamus.

Fig. 9 Effect of adding MS candidate regions obtained by a CAD system on segmentation of the white matter regions indicated by white lines: **a** without and **b** with addition of MS candidate regions obtained by the CAD system, and **c** corresponding gold standard regions. The similarity index for the white matter regions increased from 84.7% to 89.3% by use of the CAD system.

Fig. 10 Effect of removing basal ganglia and thalamus from the white matter regions indicated by white lines: **a** without and **b** with removal of the basal ganglia and thalamus regions, and **c** corresponding gold standard regions. The similarity index for the white matter regions increased from 68.2% to 84.0%.

575

576 **Fig. 11** Relationship between the average similarity indices for white matter and gray matter

577 regions.

578

579 **Fig. 12** Illustrations of brain parenchymal region (**a**, **d**), white matter regions (**b**, **e**), and gray

580 matter regions (**c**, **f**). White lines indicate output regions by the proposed method (**a**, **b**, **c**) and

581 corresponding gold standard regions (**d**, **e**, **f**). The similarity index was 95.9% for brain

582 parenchymal region and 85.7% for white matter regions.

583

Fig. 1

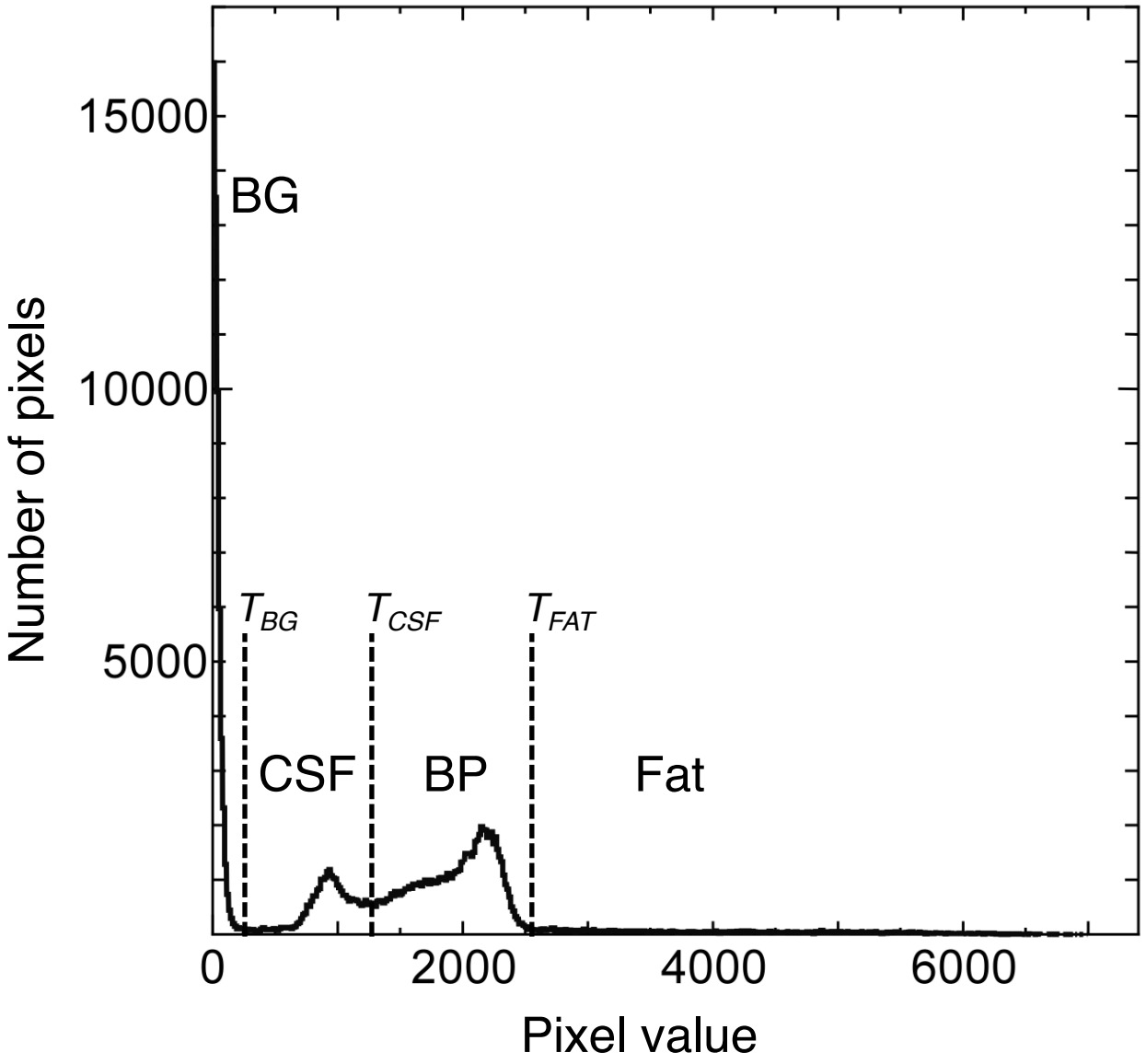
15000
10000
5000
0
2000
4000
6000
Number of pixels
Pixel value
BG
T_{BG}
T_{CSF}
T_{FAT}
CSF
BP
Fat

Fig. 2

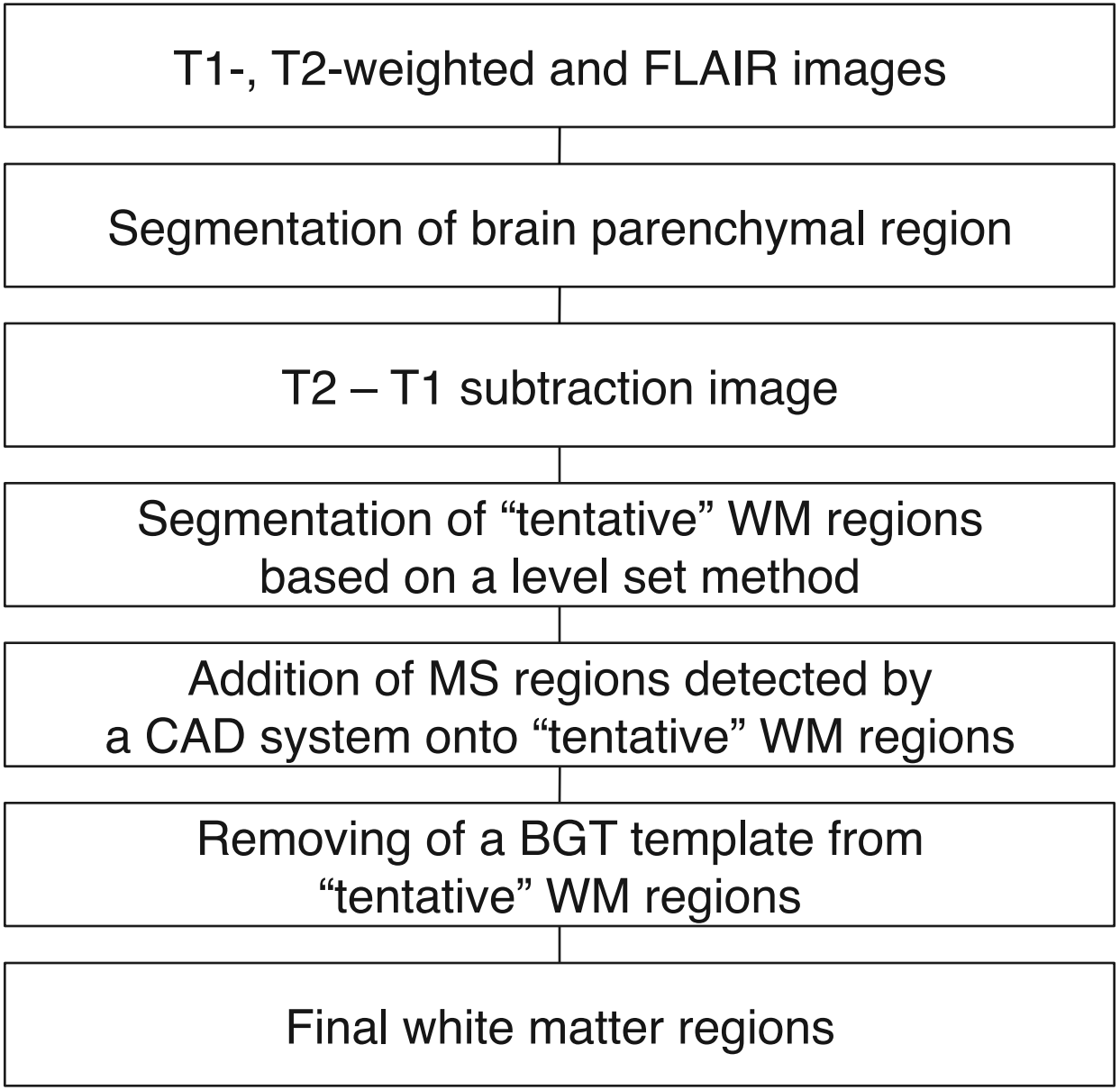
T1-, T2-weighted and FLAIR images
Segmentation of brain parenchymal region
T2 – T1 subtraction image
Segmentation of “tentative” WM regions based on a level set method
Addition of MS regions detected by a CAD system onto “tentative” WM regions
Removing of a BGT template from “tentative” WM regions
Final white matter regions

Fig. 3

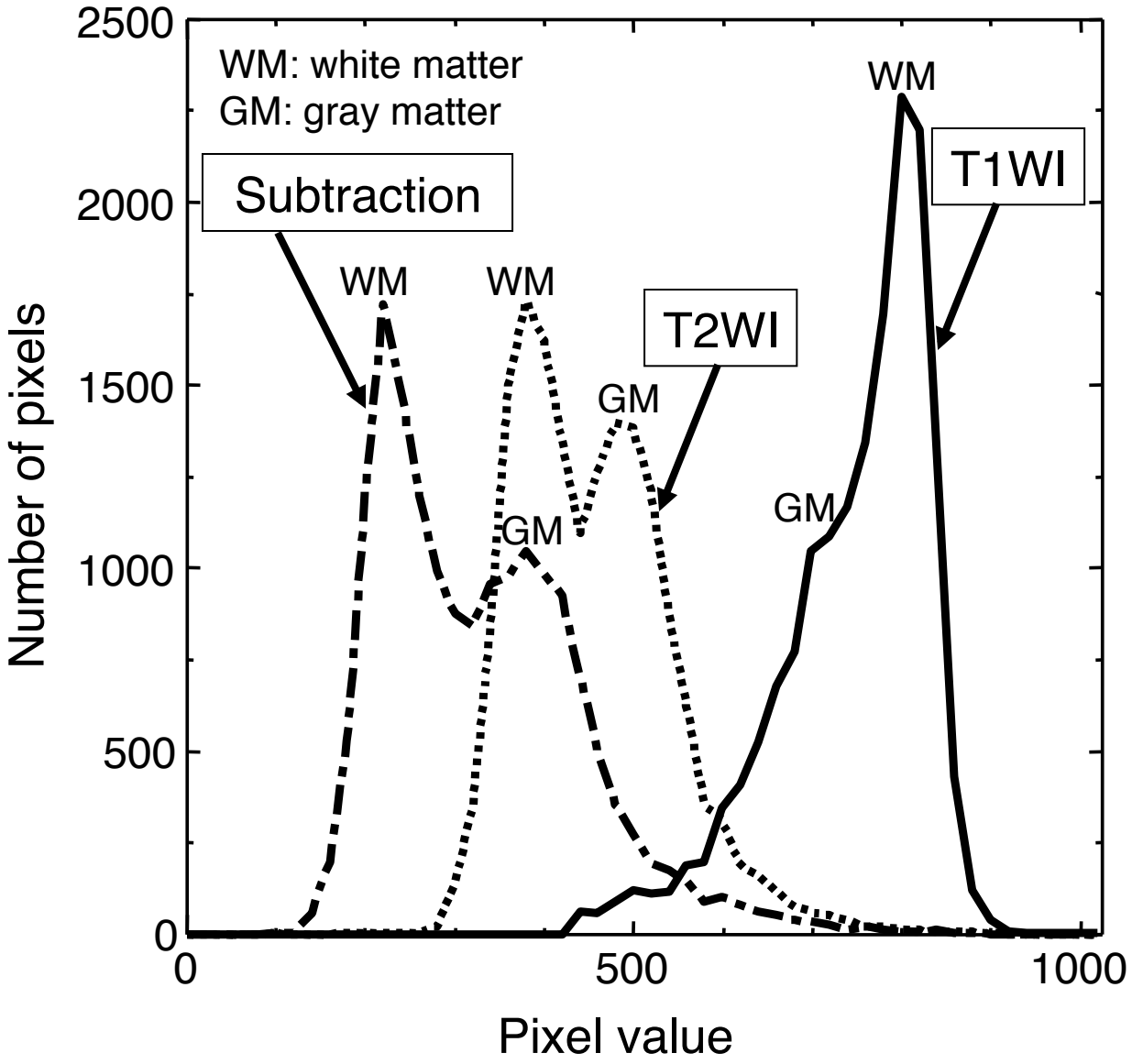
WM: white matter
GM: gray matter
Subtraction
T2WI
T1WI
WM
WM
WM
GM
GM
GM
Number of pixels
Pixel value
2500
2000
1500
1000
500
0
0
500
1000

Fig. 4

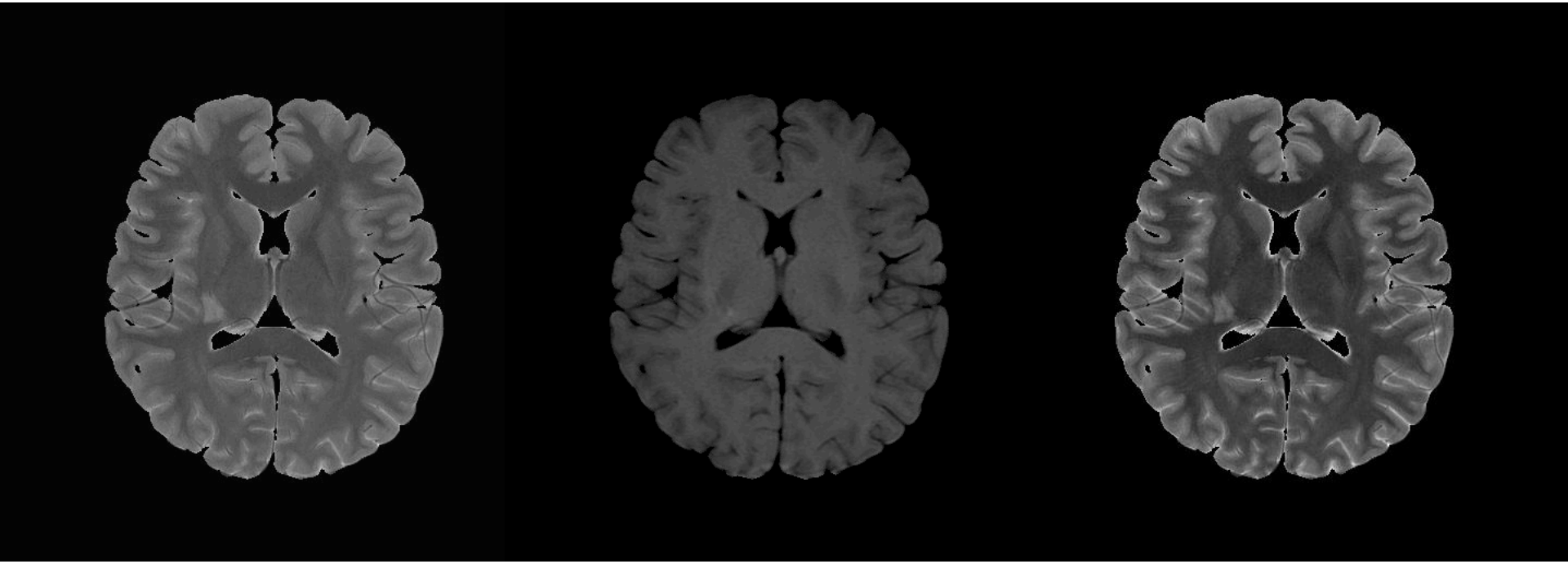

(a) (b) (c)

Fig. 5

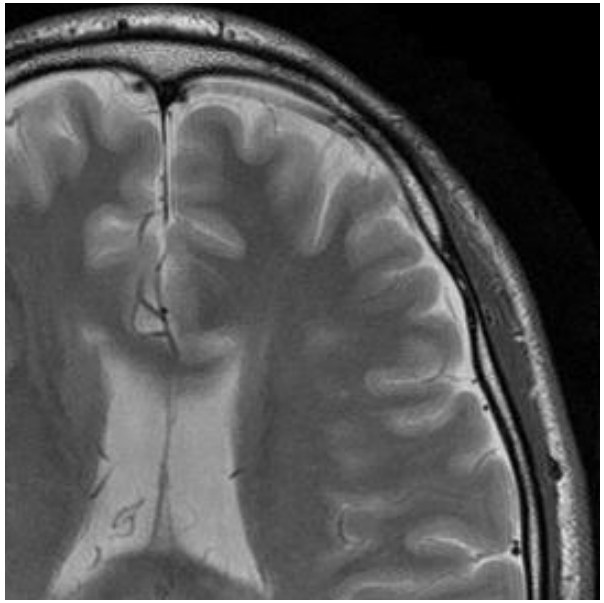

(a)

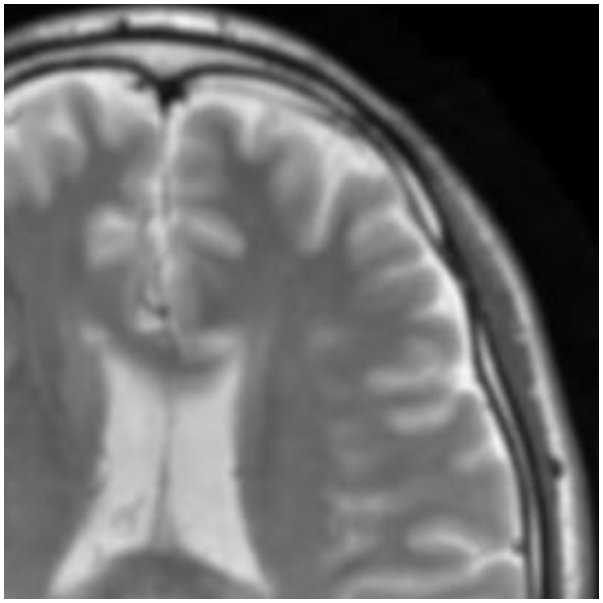

(b)

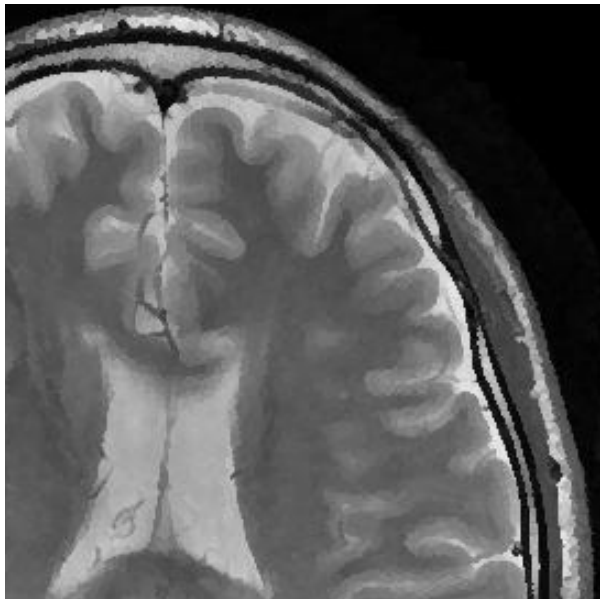

(c)

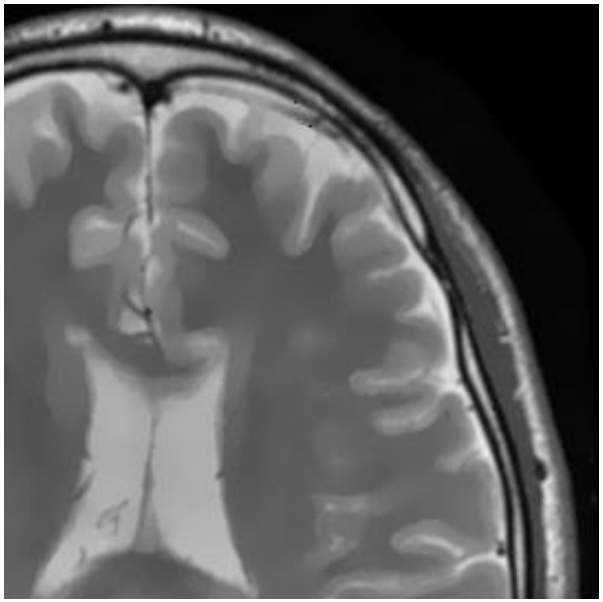

(d)

Fig. 6

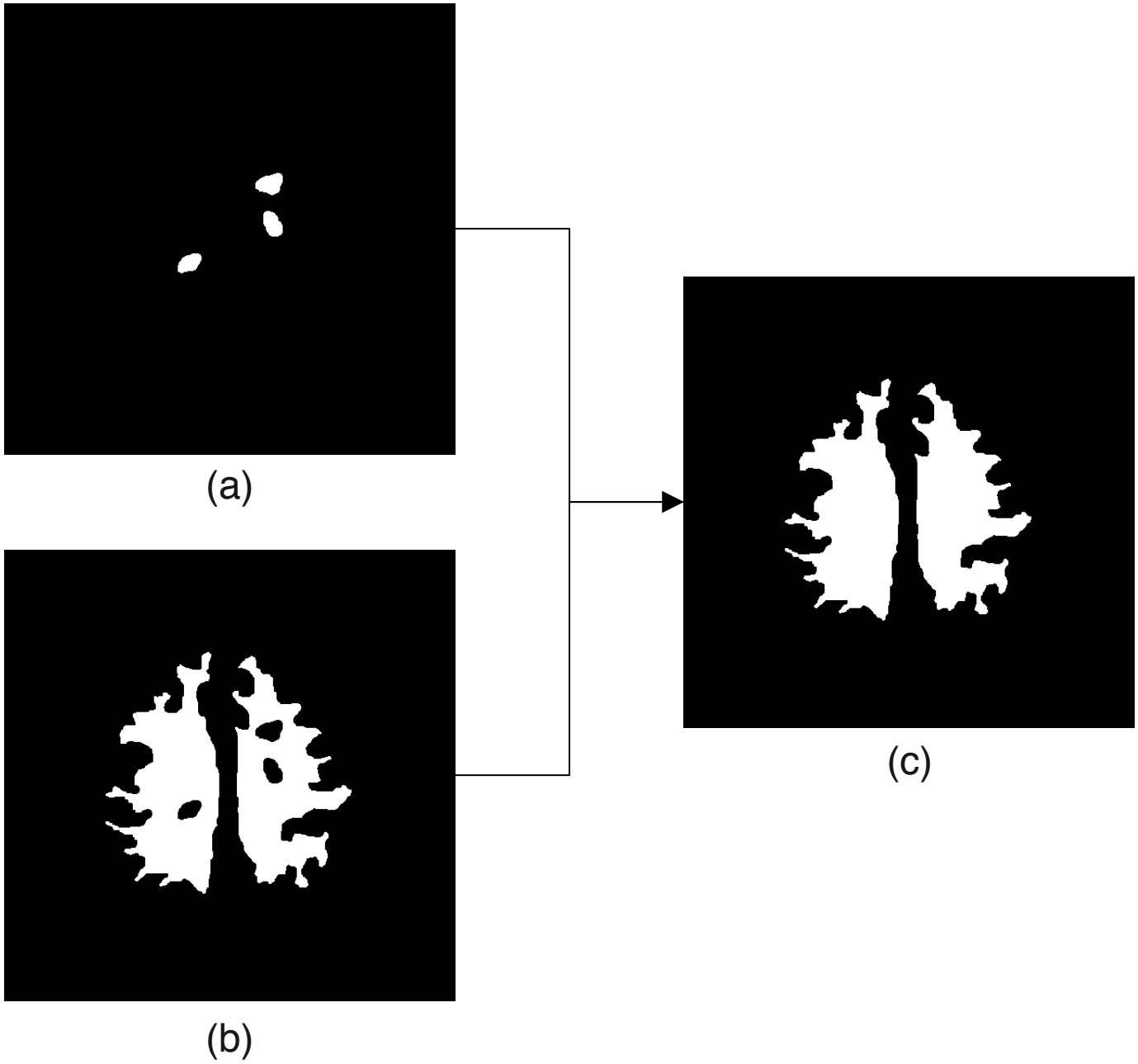

Fig. 7

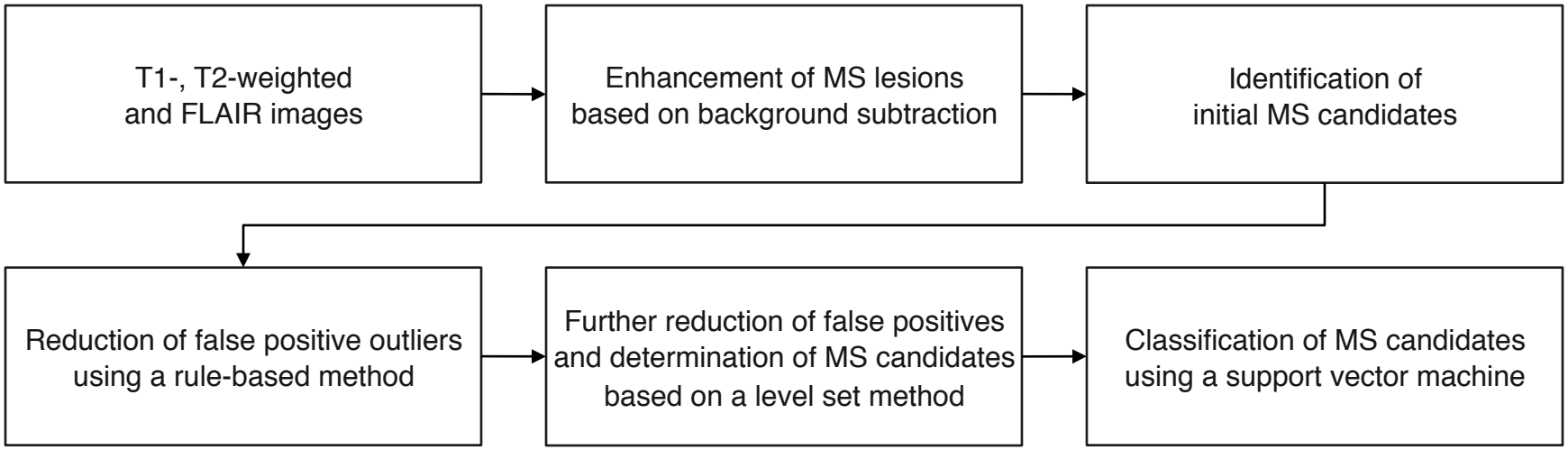
T1-, T2-weighted and FLAIR images
Enhancement of MS lesions based on background subtraction
Identification of initial MS candidates
Reduction of false positive outliers using a rule-based method
Further reduction of false positives and determination of MS candidates based on a level set method
Classification of MS candidates using a support vector machine

Fig. 8

Fig. 9

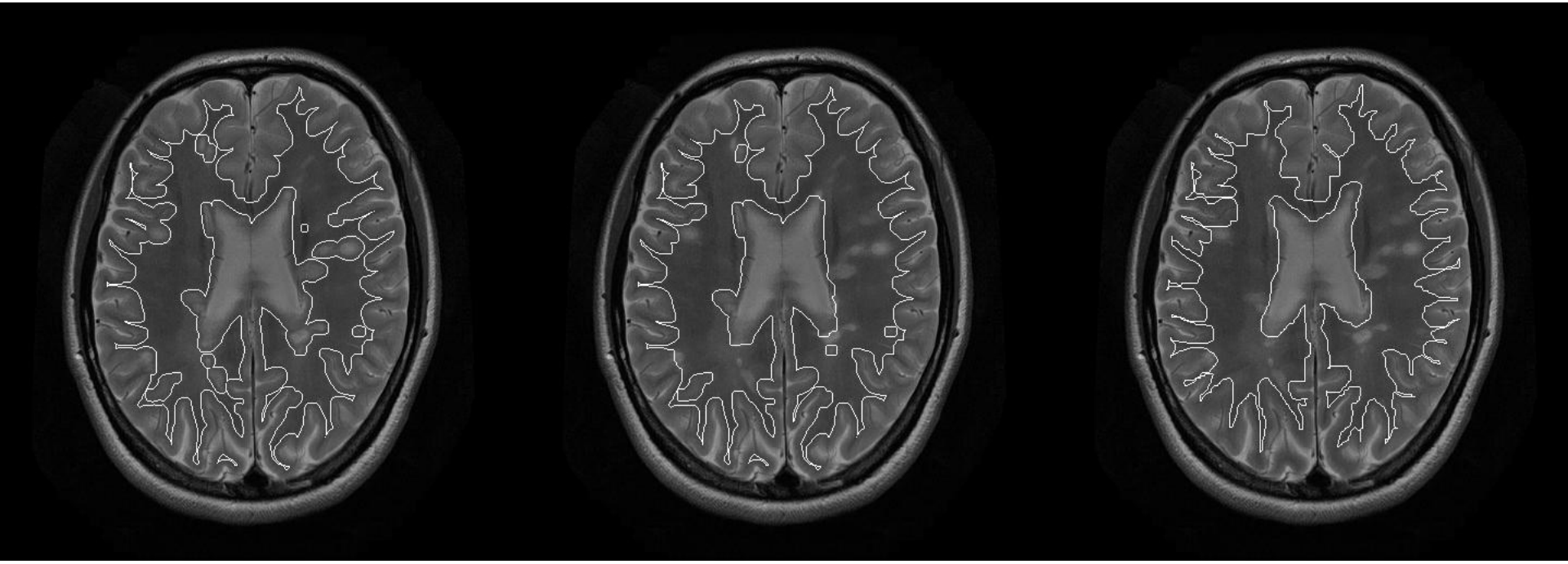

(a) (b) (c)

Fig. 10

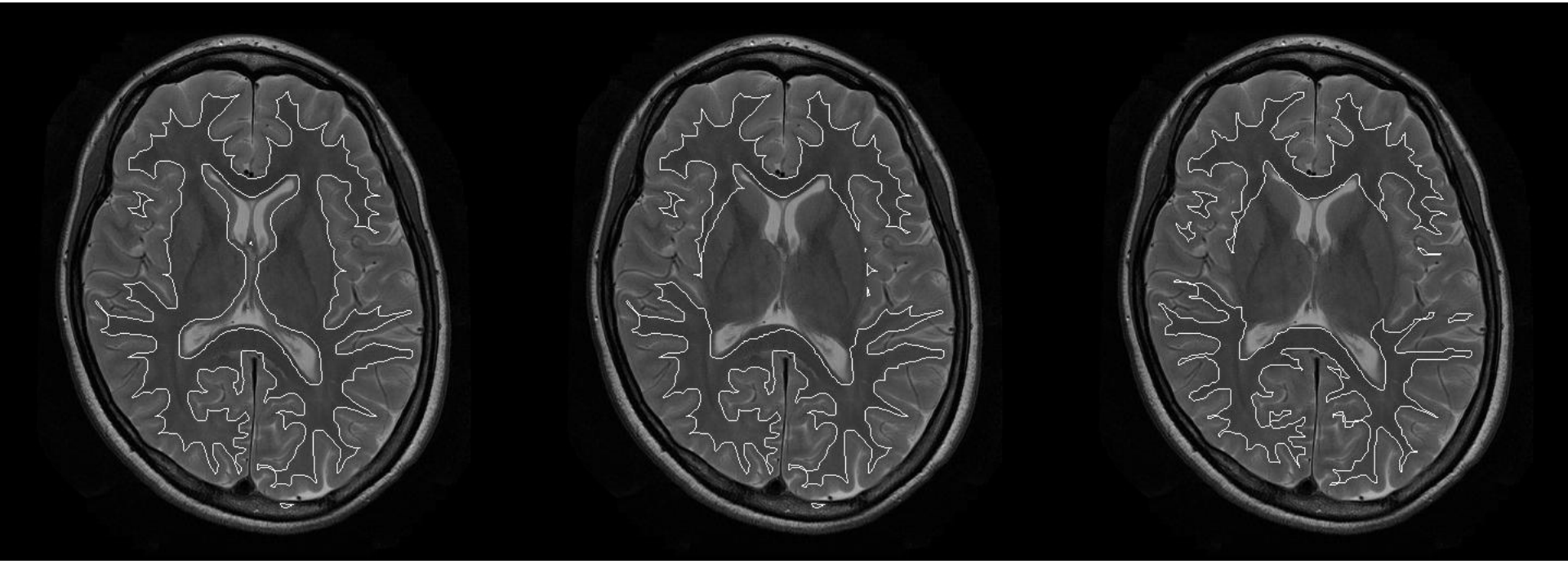

(a) (b) (c)

Fig. 11

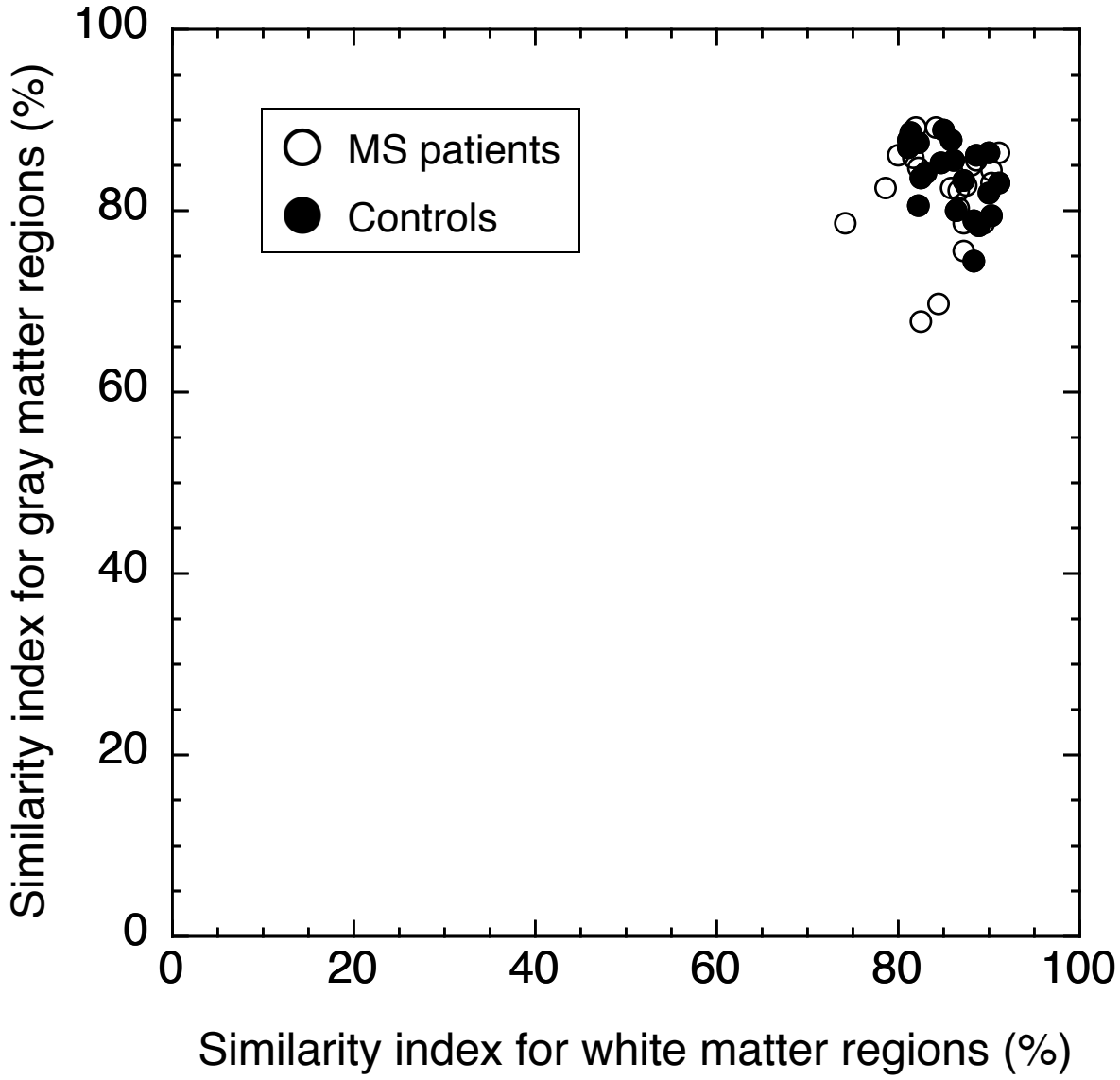
MS patients
Controls
Similarity index for gray matter regions (%)
Similarity index for white matter regions (%)
0
20
40
60
80
100

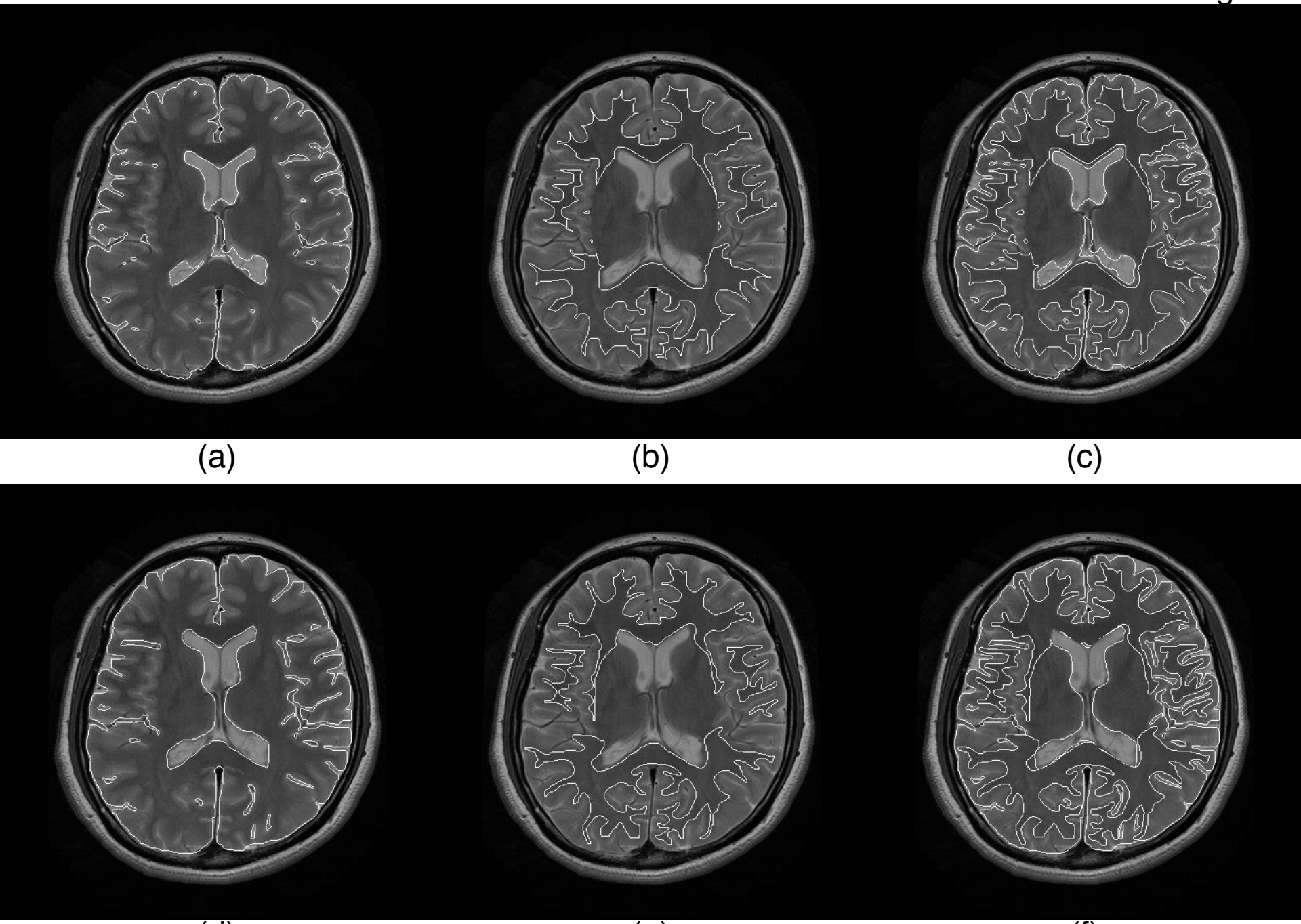
(a)
(b)
(c)
(d)
(e)
(f)